On the Formation of Multiply Coherent γ Grains in a Powder Metallurgy Ni Base Superalloy

Yonguk Lee, Cameron Hale, Eric J. Payton, and Victoria M. Miller

Abstract

In this study, a unique microstructure where γ grains contain multiple coherent primary γ′ particles is reported. We term these unique features "multiply coherent grains" (MCGs). While the γ grains containing coherent primary γ′ particles suggest the heteroepitaxial recrystallization (HeRX) mechanism, HeRX can only explain the presence of a single coherent primary γ′ within a given γ grain, not multiple. Other potential formation mechanisms of MCGs are assessed using combined energy dispersive spectroscopy and electron backscatter diffraction, then a likely formation mechanism is posited. The median grain size of MCGs surpasses other γ grains, which shows the potential impact of MCG formation on the grain size distribution.

Keywords

Powder metallurgy Ni superalloys • Heteroepitaxial recrystallization • Multiply coherent grains

Introduction

When used as turbine disk materials, Ni-base superalloys must achieve high strength at elevated temperatures for improved power and fuel efficiency. The high performance requirements of these alloys make cast and wrought processing challenging. Powder Metallurgy (P/M) is widely used as an alternative processing method, and it provides additional benefits such as less chemical segregation and a smaller grain size [1]. Turbine disks have a number of fatigue critical regions where maintaining a fine and homogeneous grain size is crucial for performance [2, 3]. One microstructural mechanism that allows the retention of a fine grain size, both during sub-solvus processing and during service, is Smith-Zener pinning by primary γ′ particles [4]. If the Smith-Zener pinning force is inhomogeneous it can result in a bimodal grain size distribution or even the formation of abnormally large grains [4, 5]. In polycrystalline Ni-base superalloy, such abnormal grains may contain long Σ3 twin boundaries, where fatigue cracks may be preferentially initiated under cyclic loading [6]. Thus, formation of coarse grains due to insufficient pinning (especially for those formed near the surface) can in some cases be tremendously detrimental for fatigue life [3, 7].

For Smith-Zener pinning to be effective, the primary γ′ particles must be located at the grain boundaries; *intragranular* primary γ′ do not contribute to the Smith-Zener pinning pressure [8]. There are three mechanisms that result in primary γ′ particles transitioning from intergranular to intragranular:

- Pinning-unpinning: the Smith-Zener pinning pressure provided by the γ′ particle is overcome by pressure driving boundary movement and the moving boundary bypasses the particle.
- Dissolution-reprecipitation: the moving boundary dissolves the particle and the local supersaturation of particle elements initiates reprecipitation as the boundary passes. Moving boundaries (such as a recrystallization front) have higher diffusivity and solubility than stationary boundaries [9], which aids in the dissolution of particles. However, dissolution becomes energetically unfavorable when particles are large, and thus, dissolution-reprecipitation is typically only observed for particles smaller than a few hundreds nanometers in diameter [10].
- Heteroepitaxial recrystallization (HeRX): a γ phase recrystallization nucleus coherently templates off an existing primary γ′ particle [11].

Y. Lee (✉) · C. Hale · V. M. Miller
Department of Materials Science and Engineering, University of Florida, Gainesville, FL 32611, USA
e-mail: leey2@ufl.edu

E. J. Payton
Department of Materials Science and Engineering, University of Cincinnati, Cincinnati, OH 45219, USA

J. Cormier et al. (eds.), *Superalloys 2024*, The Minerals, Metals & Materials Series,
https://doi.org/10.1007/978-3-031-63937-1_73

Each of the mechanisms results in unique microstructures. A γ grain formed via either pinning-unpinning or dissolution-reprecipitation can have *multiple* internal particles while heteroepitaxial recrystallization (HeRX)-γ only has a single internal particle. The size, shape, and orientation of particles stay fairly intact during pinning-unpinning, however, they drastically change when dissolved and reprecipitated.

In a recently published study by the authors [12], a microstructure not completely explained by the aforementioned mechanisms was observed in which multiple micron-sized, and coherent γ′ particles were located inside of a single γ grain. We have termed these features "multiply coherent grains" (MCGs). Surveying the literature, similar microstructures have been observed in at least one other instance [13]. The objective of the present study is to explain the formation mechanism of these MCGs.

Material and Methods

The P/M low solvus high refractory (LSHR) alloy material used in this work was originally characterized in Reference [14], then further characterized as part of the present authors' larger study [12]. The key experimental methods are summarized here. LSHR has an intermediate lattice misfit; it is measured as 0.23 % at room temperature [15] and is predicted to increase as temperature increases [16]. The occurrence of HeRX in LSHR system was observed and reported recently even though a high lattice mismatch had been considered a hurdle for that mechanism [12].

Double cone compression specimens were fabricated using electro-discharge machining (EDM), which does not change microstructure during fabrication but enables to build a range of strains (0–1.0) during compression. Starting with the as-received billet microstructure, the specimen was isothermally forged at 1065 °C (below the γ′-solvus, 1157 °C) at an initial plastic strain rate of 0.1 /s. Prior to deformation, the specimen was held for 5 min at the forging temperature. At the conclusion of deformation, the specimen was immediately water quenched.

Due to the nature of the double cone geometry, a range of strain rates and strains is produced across the radius of the specimen. Details of the gradient of strain rates and strains across the specimen can be found in Reference [12]. While adiabatic self-heating is possible, it is typically only problematic at high strain rates over 1/s [17]. The effect of self-heating in this study is expected to be negligible.

Radial sections of the as-forged microstructure were prepared for microstructural characterization by grinding with successively finer silicon carbide abrasive papers, followed by polishing with a 1 μm alumina suspension and finally vibratory polishing using a 0.05 μm colloidal silica suspension. Microstructural characterization was completed using simultaneous electron backscatter diffraction (EBSD) and energy dispersive spectroscopy (EDS) at 15 kV operating voltage and 13 nA beam current with a 0.25 μm step size. The combined technique is necessary because EBSD alone cannot differentiate between γ and γ′ due to the similarity in crystal symmetry; instead, chemistry information from EDS is used to differentiate between the phases [18]. Due to the large interaction volume of EDS, only large primary γ′ particles (> ~1 μm diameter) were unambiguously identified. Secondary or tertiary γ′ were undetected, resulting in a γ′ volume fraction which is lower than expected from the material chemistry.

The open-source MATLAB package MTEX [19] was used for the post-processing of EBSD-EDS data, calculation of grain information, and figure generation. The misorientation threshold used for coherency in this study is 3°, though the results were insensitive to this value. The threshold for general grain segmentation used in this study was 5°.

Results and Discussion

A representative microstructure of interest in this study is presented in Fig. 1. The microstructure was taken from the mid-radius region where the final compressive plastic strain was 0.2. The coherent boundaries between primary γ′ particles and γ matrix are colored in white in the inverse pole figure (IPF), as shown in Fig. 1a. With a prevalent HeRX-γ, populations of γ grains that contain *multiple* coherent primary γ′ particles are present. Such γ grains with multiple coherent primary γ′ particles will be referred to as multiply coherent grains (MCGs).

The possibility that the apparent MCGs result from stereology (i.e., the *appearance* of multiple particles is caused by the section plane of one large sub-surface particle with complex morphology) was considered. However, stereology is unlikely to be the cause of the MCGs because some of the similarly orientated particles are multiple microns apart. This would require an implausibly large sub-surface particle. In fact, it is more likely that stereological considerations cause the under-reporting of MCGs, as the section plane must intersect both particles within the γ grain.

As shown in the grain average misorientation (GAM) map in Fig. 1b, MCGs (with bold outlines) have minimal internal misorientation, which means they were likely formed via dynamic recrystallization during hot compression. Several of the MCGs have an internal low angle boundary separating the coherent primary γ′ particles. MCGs were observed across the whole range of plastic strains (0.1–1) across the radius of the specimen.

The presence of a coherent interface between a primary γ′ particle and its surrounding γ grain suggests the activity of HeRX. However, the formation of MCGs cannot be fully explained with the current understanding of HeRX, as

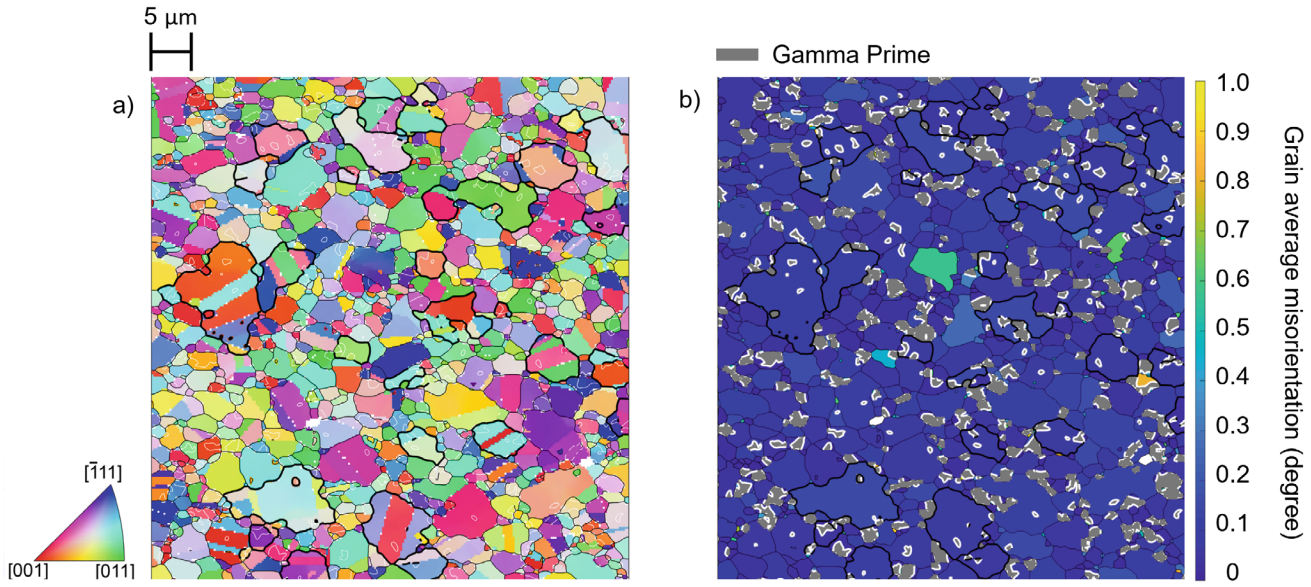

Fig. 1 **a** Inverse pole figure (IPF) map with reference direction out of the plane of the page. White boundaries indicate a coherent interface, while black boundaries denote conventional grain boundaries. **b** Grain average misorientation (GAM) of each grain. Low GAM of MCGs indicates the grains are likely recrystallized. In both the IPF map and GAM map, MCGs are highlighted with a bold outline

it proposes one γ grain nucleating off one primary γ′ particle [11, 20]. This standard description does not include a mechanism in which multiple primary γ′ would occur inside a single recrystallized γ grain. Other potential formation mechanisms are considered in the next section.

Potential Mechanisms of MCGs Formation

The formation of MCGs requires groups of primary γ′ particles having the same orientation; however, it is uncertain whether these groups pre-exist in the microstructure or form during the most recent iteration of recrystallization. Phrased another way, did the recrystallization front move past the primary γ′ particles via a pinning-unpinning mechanism or via a dissolution-reprecipitation mechanism? Based on this, the authors examined two possible mechanisms for the formation of MCGs: 1) the moving recrystallization front "cut" the primary γ′, with the moving boundary dissolving and reprecipitating them, or 2) the spatial correlation of similarly oriented primary γ′ preceded recrystallization and formed earlier in processing.

The first potential scenario for the formation of MCGs is dissolution-reprecipitation or the particle cutting mechanism. When the moving boundary, such as the recrystallization front, passes through second phase particles, it can dissolve the particles and result in local supersaturation of particle elements. This provides the driving force to reprecipitate the secondary phase behind the moving boundaries (dissolution-reprecipitation). In some cases there is no time delay between the dissolution and reprecipitation, leading to the boundary apparently "cutting" and reorienting the particle to be coherent with the γ front as it passes [9]. If the recrystallization front encountered and cut through several primary γ′ particles, it could result in an MCG-like microstructure. However, particle cutting has only been observed under narrow ranges of thermo-mechanical processing conditions, particularly slow strain rates, and only for secondary and tertiary precipitates [21, 22]. As the energy required to dissolve and reprecipitate a particle scales volumetrically [10], the energy penalty of cutting the particle increases rapidly with particle size. Additionally, the strain rates used in this study are higher than those where particle cutting is typically reported. This makes it unlikely that particle cutting is responsible for the MCGs observed herein, though it cannot be definitively ruled out.

The second possible formation mechanism of MCGs is that clusters of similarly oriented primary γ′ pre-existed in the microstructure before the thermo-mechanical processing. If the oriented clusters of primary γ′ pre-existed in the microstructure, HeRX nucleation could occur at one (or more) of the particles. This would result in a recrystallization front that has the same crystallographic orientation as the surrounding particles. If the recrystallization front bypasses these particles by pinning-unpinning, it would result in an MCG structure. This proposed formation mechanism is illustrated in Fig. 2. The authors assert that this is the most likely formation mechanism of MCGs.

The second possible formation mechanism for MCGs is that pre-existing clusters of similarly oriented primary γ′ are

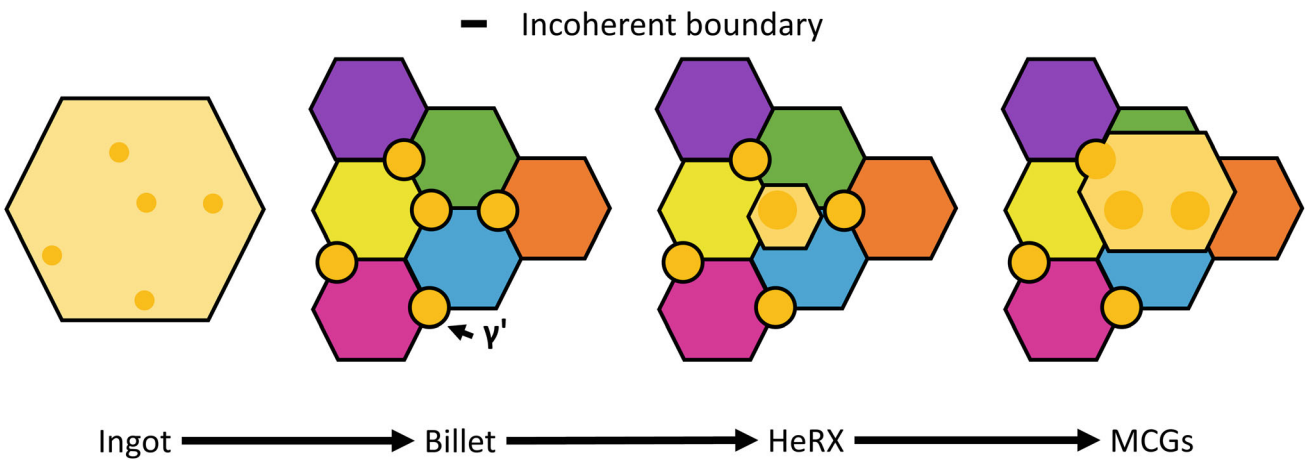

Fig. 2 Schematic diagram illustrating the proposed mechanism of MCG formation. During ingot-to-billet processing, primary γ′ are coarsened but their local orientation is biased. Following sub-solvus hot deformation initiates HeRX nucleation from one γ′ particle. Finally, the growth of the HeRX grain forms MCGs

already present in the microstructure. This was tested by quantifying the spatial correlation of primary γ′ below a misorientation threshold of 3°. Any two γ′ particles with a misorientation below the threshold were counted as a 'pair' and the separation distance was recorded, then the distribution of distances was plotted in Fig. 3. For comparison, the locations/orientations of the γ′ particles were randomly shuffled and the distances between similarly oriented γ′ particles were again calculated. As shown, clustering in the "real" microstructure manifests as small spacings between similarly oriented γ′. Comparison with the randomized structure (rather than *e.g.,* the starting microstructure) allows for any texture of the γ′ particles to be accounted for. This methodology is an analog to "correlated" and "uncorrelated" misorientation distribution functions often used to quantify grain boundary character [23–25]. Both the original and the randomized distributions are plotted in Fig. 3a.

The real and randomized microstructures have notably different spatial correlations of primary γ′ particles. A random distribution of γ′ orientations (without any clustering) results in more 'pairs' of similarly oriented γ′ particles with increasing distance, as the sample area and number of particles observed increases with distance. In reality, imaged areas have finite sizes, so the randomized distribution (blue) has a peak with the decrease at large separations due to the boundaries of the measured region. In contrast, the real distribution in the sample shows strong clustering; there is a tremendous peak at the radial centroid-to-centroid distances of less than 5 microns.

While Fig. 3a illustrates the presence of γ′ orientation clusters, it includes the grains already identified as MCGs. In Fig. 3b, the above analysis is repeated but grains already identified as potential HeRX grains (or MCGs) due to a coherent γ-γ′ interface are excluded. As shown, the clustering is still present; groups of similarly oriented primary γ′ extend past the boundaries of existing MCGs. Therefore, the presence of the clusters must have preceded the current stage of processing, i.e., the particles of similar orientation were already clustered in the starting material due to some prior processing stage.

Though identification of the formation mechanism of these oriented particle clusters is beyond the scope of the present manuscript, the cluster sizes are consistent with feature sizes characterized during prior processing. As reported by Semiatin *et al.*, this LSHR billet was formed via powder extrusion with a reported powder size of 23 μm [14]. The largest clusters within the peak are approximately 8 μm in separation, which is consistent with the grain sizes in polycrystalline powder. It is possible that the primary γ′ particles observed during this stage of processing are over-grown precipitates originating from a single grain within a powder particle.

More broadly, there are a number of mechanisms by which clusters could form. Clusters of similar orientation γ′ particles have been reported in Ni-base superalloys that undergo ingot-to-billet processing (such as LSHR) in which recrystallization is not complete at the early stage super-solvus thermo-mechanical processing [26]. Under these bimodal stored energy conditions, recrystallized grains can grow into the neighboring unrecrystallized grains. The recrystallization front would encounter γ′ small enough to be reoriented by dissolution-reprecipitation (due to the effects of super-solvus processing). This results in nearly coherent- or twin-orientation $\gamma - \gamma'$ [26, 27]. In other words, the orientation of those intragranular γ′ becomes significantly biased locally. Such an ingot condition is illustrated in Fig. 2. The following sub-solvus billet conversion processing can result in the coarsening of the γ′ and recrystallization of new γ grains near the γ′ that do not have an orientation relationship to the particles.

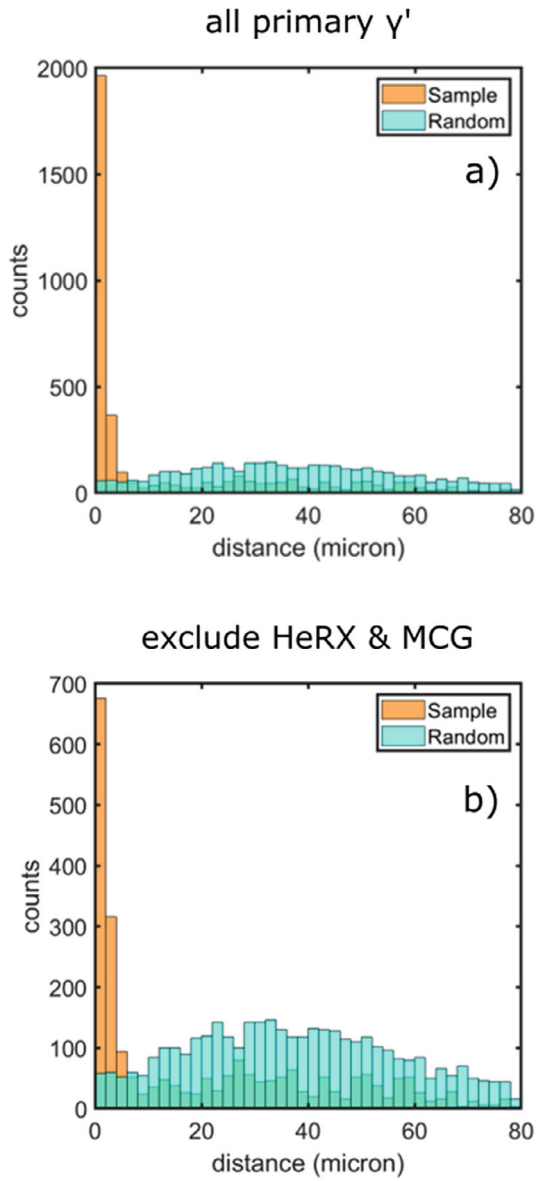

Fig. 3 Histograms plotting the number of pairs of similarly oriented primary γ' as a function of separation distance. **a** Counts every instance of two γ' particles being similarly oriented. **b** Excludes the counting of γ' particles which are contained within any HeRX grain or MCG

To summarize, microstructural evidence suggests that the orientation clusters of primary γ' particles pre-existed in the microstructure prior to the deformation processing in this study. To form MCGs, HeRX first occurs at one primary γ' within a cluster. As the HeRX γ grain grows, the recrystallization front encounters other similarly oriented γ' particles within the cluster. Due to the similarity in orientation, the recrystallizing γ can form an interface that is at least partially coherent. In other instances, HeRX nucleation may occur at 2 or more γ' particles in an orientation cluster. These nuclei would merge into a single grain upon impingement.

Notably, when a recrystallization front encounters a particle of nearly the same orientation, the ability to form a (semi)coherent interface reduces the effect of Smith-Zener pinning. There is a "wicking" force which draws the recrystallization front around the particle, discussed further below.

Modified Smith-Zener Pinning Force

The modification to conventional Smith-Zener pinning was calculated for a recrystallization front growing into an oriented particle cluster. In its most basic form, the Smith-Zener expression describes the force acting against a growing grain boundary front, as given by

$$F_Z = 2\pi r\ \gamma_{GB}\ sin\theta\ cos\theta\ \left[\frac{J}{m}\right] \tag{1}$$

where r is the particle radius, γ_{GB} is the grain boundary energy, and θ is the dihedral angle formed where a grain boundary meets the particle surface. θ represents how far the boundary has swept through the particle. This setup is shown schematically in Fig. 4a. The conventional Zener calculation balances this drag pressure and the driving pressure for boundary movement.

In this conventional form, the particle is incoherent (i.e., has a high-energy interface) with both grains, so when the boundary intersects the particle it reduces the total energy. Another derived form assumes that the particle is initially coherent with its host grain, so the advancing boundary replaces a low-energy interface with a high-energy interface [28]. Under these assumptions, the pinning force is doubled. In the present case of MCGs, the case is reversed: a new low-energy coherent particle-matrix interface is created as the boundary advances.

With this new assumption, the pinning force can be rederived. First, the area of particle interface converted from incoherent to coherent can be described by the spherical cap equation:

$$A = 2\pi r^2(1 - cos(\phi))\ [m^2] \tag{2}$$

where r is the radius of the particle and ϕ is the angle between the rays from the center of the sphere to the apex of the cap and the edge of the disk forming the base of the cap. As shown in Fig. 4a, ϕ is the complementary angle to the θ used in the Smith-Zener equation. The spherical cap equation can be rewritten in terms of θ:

$$A = 2\pi r^2(1 - cos(\pi/2 - \theta))\ [m^2] \tag{3}$$

The associated energy for this new interfacial area will be the difference in interfacial energy over the length of the

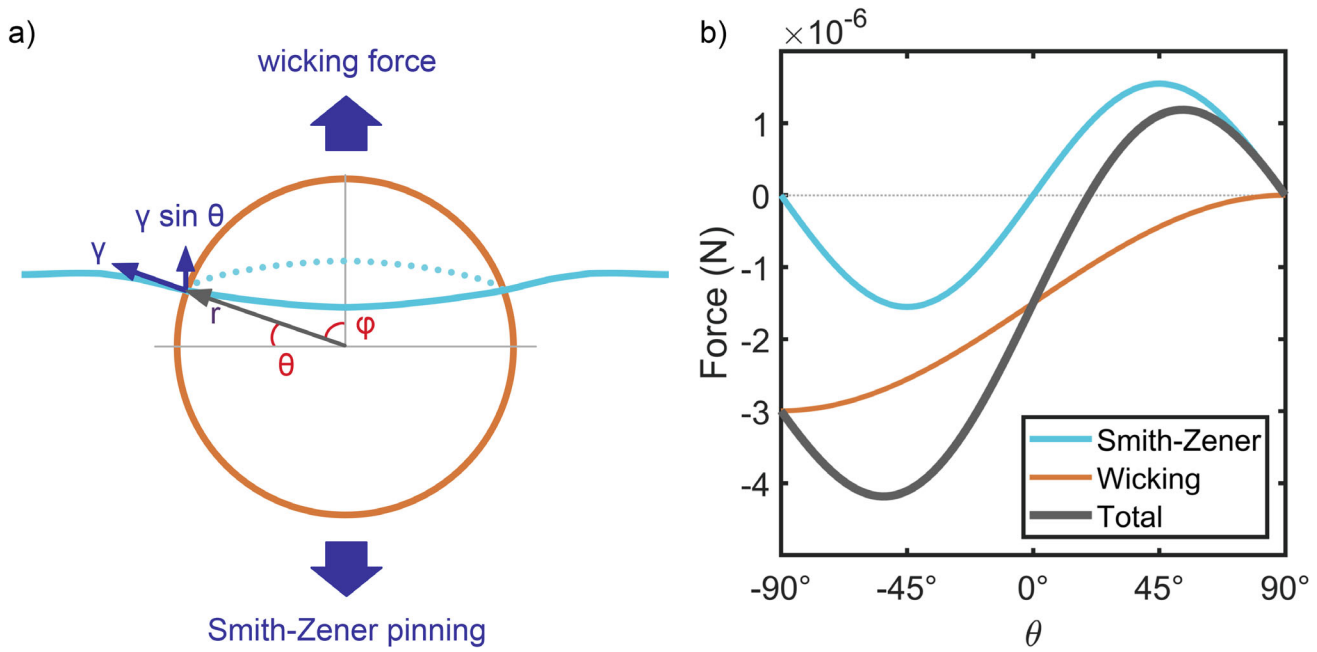

Fig. 4 Pinning force as a function of dihedral angle-θ. **a** Schematic diagram which describes how far the boundary has swept through the particle. **b** Components and total pinning force as a function of θ. The wicking force is always negative, which reduces the pinning force across the entire particle

grain boundary within the particle (approximated by particle diameter),

$$Interfacial\ Component = (\gamma_{coherent} - \gamma_{incoherent})/(2r)\left[\frac{J}{m^3}\right] \tag{4}$$

where γ is the interfacial energy and r is the particle radius. The total energy is achieved by multiplying this energy component by the new interfacial area described in the spherical cap equation:

$$F_w = 2\pi r^2(1 - cos(\pi/2 - \theta)) * ((\gamma_{coherent} - \gamma_{incoherent})/(2r))\left[\frac{J}{m}\right] \tag{5}$$

As incoherent interfacial energies can be assumed to be higher than coherent interfacial energies in a given material, this term will be negative (favorable). Simplification of the terms in this equation:

$$F_w = (\gamma_{coherent} - \gamma_{incoherent})\pi r(1 - cos(\pi/2 - \theta))\left[\frac{J}{m}\right] \tag{6}$$

The additional "wicking" force can be incorporated into the Smith-Zener pinning force:

$$F_{Total} = F_Z + F_w = (2\pi r\gamma_{GB} sin\theta cos\theta) + (\gamma_{coherent} - \gamma_{incoherent})\pi r(1 - cos(\pi/2 - \theta))\left[\frac{J}{m}\right] \tag{7}$$

Simplification results in the following equation for the total force:

$$F_{Total} = F_Z + F_w = (2\pi r\gamma_{GB} sin\theta cos\theta) + \pi r(\gamma_{coherent} - \gamma_{incoherent})(1 - cos(\frac{\pi}{2} - \theta))\left[\frac{J}{m}\right] \tag{8}$$

Figure 4b illustrates the components and total pinning force as a function of θ.

The conventional Smith-Zener component is initially negative as more and more boundary area is removed from the system. A maximum pinning force is seen at 45°. The wicking force is always negative, favoring the advancement of the boundary. The total pinning force (including wicking) has a reduced maximum pinning force, and the maximum occurs at a larger angle, 49.8°. The reduction in pinning efficacy would be manifested in the microstructure through larger grain sizes.

Potential Impact of MCGs Formation on GSD

Further implication of reduced Smith-Zener pinning on the formation of MCGs and resulting microstructure is investigated by comparing grain size distribution of each type of γ grains. The effective grain size distributions for γ grains (no coherent γ′interfaces), HeRX grains (coherent interface with one γ′ particle) and MCGs (coherent interfaces with multiple γ′particles) are compared in Fig. 5. The plotted grain sizes are equivalent circular diameters where an HeRX γ-γ′ pair is treated as a single grain.

The HeRX grains and matrix grains have similar median sizes. The spread in matrix γ sizes appears larger; however, it is possible that this results from stereological effects. For an HeRX grain to be detected and correctly classified, the section plane must pass through the γ′ particle to illustrate the coherent interface. Many section planes in HeRX grains will intersect an insufficient volume of the associated γ′ particle for accurate EDS classification, resulting in over-reporting of matrix γ grains. This stereological effect likely contributes to the difference in apparent distribution widths between the HeRX grains and other γ grains.

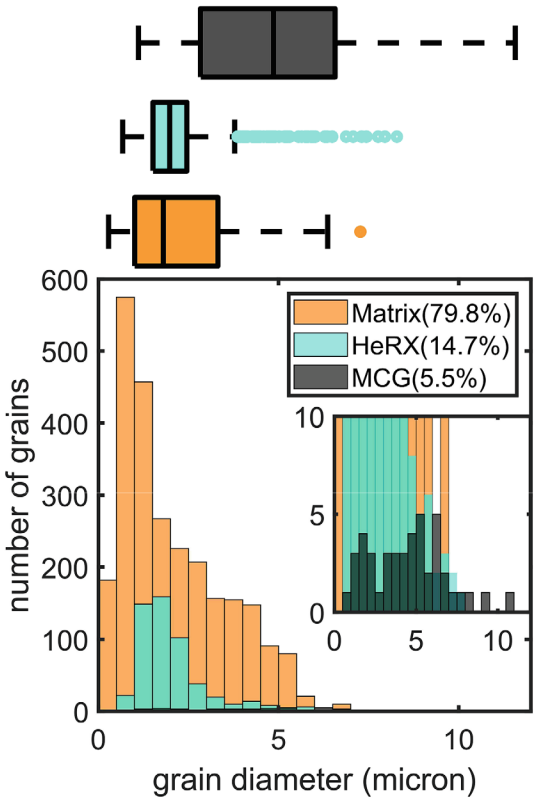

Fig. 5 Histogram and box plot displaying the grain diameter and number of occurrences of MCG, HeRX, and Matrix grains. The legend shows the percentage of the total area that each category represents. Multiply coherent grains are the largest in the microstructure with a median grain size significantly larger than either HeRX or matrix grains

Table 1 Predicted maximum grain size using conventional Zener pinning calculations (d_Z) and Zener pinning plus wicking calculations (d_{Z+W}) for varying particle distributions. The baseline condition is representative of the material used in this study

	V_f (%)	γ′ radius (μm)	d_Z	d_{Z+W}
Baseline	13	0.57	11.70	15.52
Larger γ′	13	1.00	20.52	27.24
Larger V_f	20	0.57	7.60	10.08
Larger γ′& V_f	20	1.00	13.34	17.70

Conversely, the MCGs have a median diameter that is substantially larger than either the matrix γ or HeRX grains, with a median diameter of 5.6 μm as compared to 1.9 and 2.0 μm. The MCGs account for 2 % of the grains based on number fraction, but account for nearly 11 % of the measured area. While the number of MCGs measured is obviously lower than the number of HeRX or matrix γ grains, it is statistically likely that they are from a different distribution. Their larger size can be at least partially attributed to the reduction in the Smith-Zener pinning force.

For both HeRX and MCGs, stereological effects may affect the quantification of volume fraction. In both cases, the section plane must cross the coherent γ′ particle(s) for the HeRX grain or MCG to be counted. As such, the included quantification should be considered a lower bound estimate.

To further illustrate the role of the reduced pinning force and how it may be magnified during subsequent solution treatment, the Zener-limited grain diameter [10] was calculated under the assumptions of conventional Smith-Zener pinning and pinning modified with a wicking force. The results are presented in Table 1. Different combinations of γ′ size and volume fraction are considered. While these are idealized theoretical cases, they illustrate that even the relatively modest reduction in pinning efficacy from the wicking force can result in substantial increases in the average grain diameter.

Conclusions

In summary, the origins and implications of multiply coherent grains (MCGs) were investigated for the first time. Potential mechanisms for their formation were examined, and the potential role of MCGs in microstructural evolution was discussed. The following conclusions can be drawn:

- Recrystallized γ grains containing multiple coherent primary γ′ particles were described for the first time and termed “multiply coherent grains” (MCGs).

- The formation of MCGs most likely results from HeRX on one or more γ' particles in a pre-existing cluster of similarly oriented primary γ' particles.
- MCGs are substantially larger in diameter than either matrix γ grains or other HeRX grains.
- The large size of MCGs can be partially attributed to reduced efficacy of Smith-Zener pinning when a grain encounters a particle with which it can form a low-energy coherent interface.

Acknowledgements This material is based upon work supported by the National Science Foundation under Grant No. DMR-2042287. This work was performed in part at the Analytical Instrumentation Facility (AIF) at North Carolina State University, which is supported by the State of North Carolina and the National Science Foundation (award number ECCS-2025064). The AIF is a member of the North Carolina Research Triangle Nanotechnology Network (RTNN), a site in the National Nanotechnology Coordinated Infrastructure (NNCI). The authors would like to acknowledge P. Fagin (AFRL and UES, Inc.) for assistance with mechanical testing, and Brady Dowdell (NCSU) for the collection of the original EBSD data. A portion of this work was supported by the Metallic Materials and Processing Program at the Air Force Research Laboratory Materials and Manufacturing Directorate.

Conflict of Interest The authors declare that they have no conflict of interest.

References

1. S. Tin, T. Pollock, Turbine Aerodynamics, Heat Transfer, Materials, and Mechanics, volume 243, American Institute of Aeronautics and Astronautics, Inc., Reston, VA, 2014. _eprint: https://arc.aiaa.org/doi/pdf/10.2514/4.102660.
2. D. J. Morrison, J. C. Moosbrugger, Effects of grain size on cyclic plasticity and fatigue crack initiation in nickel, International Journal of Fatigue 19 (1997) 51–59.
3. J. Miao, T. M. Pollock, J. Wayne Jones, Microstructural extremes and the transition from fatigue crack initiation to small crack growth in a polycrystalline nickel-base superalloy, Acta Materialia 60 (2012) 2840–2854.
4. M.-A. Charpagne, J.-M. Franchet, N. Bozzolo, Overgrown grains appearing during sub-solvus heat treatment in a polycrystalline γ – γ' Nickel-based superalloy, Materials & Design 144 (2018) 353–360.
5. V. Miller, E. Payton, A. Pilchak, Reduction in the thermodynamic nucleation barrier via the heteroepitaxial recrystallization mechanism, Scripta Materialia 136 (2017) 128–131.
6. J. Prouteau, P. Villechaise, L. Signor, J. Cormier, Early Stages of Fatigue Crack Initiation in Relation With Twin Boundaries in Polycrystalline Ni-Based Superalloy AD730™, Metallurgical and Materials Transactions A 54 (2023) 1998–2010.
7. B. Flageolet, O. Yousfi, Y. Dahan, P. Villechaise, J. Cormier, Characterization of Microstructures Containing Abnormal Grain Growth Zones in Alloy 718, in: Superalloy 718 and Derivatives, John Wiley & Sons, Ltd, 2010, pp. 594–606. _eprint: https://onlinelibrary.wiley.com/doi/pdf/10.1002/9781118495223.ch46.
8. K. Song, M. Aindow, Grain growth and particle pinning in a model Ni-based superalloy, Materials Science and Engineering: A 479 (2008) 365–372.
9. A. Porter, B. Ralph, The recrystallization of nickel-base superalloys, Journal of Materials Science 16 (1981) 707–713.
10. F. Humphreys, M. Hatherly, Recrystallization and related annealing phenomena, Pergamon, Oxford, 2004.
11. M.-A. Charpagne, T. Billot, J.-M. Franchet, N. Bozzolo, Heteroepitaxial recrystallization: A new mechanism discovered in a polycrystalline γ – γ' nickel based superalloy, Journal of Alloys and Compounds 688 (2016) 685–694.
12. Y. Lee, E. Hershkovitz, H. Kim, K. N. Wertz, E. J. Payton, V. M. Miller, Prevalence of Heteroepitaxial Recrystallization in the Low Solvus High Refractory (LSHR) γ – γ' Superalloy, Metallography, Microstructure, and Analysis (2024).
13. E. Payton, Characterization and Modeling of Grain Coarsening in Powder Metallurgical Nickel-Based Superalloys, PhD dissertation, The Ohio State University, 2009.
14. S. L. Semiatin, K. E. McClary, A. D. Rollett, C. G. Roberts, E. J. Payton, F. Zhang, T. P. Gabb, Microstructure Evolution during Supersolvus Heat Treatment of a Powder Metallurgy Nickel-Base Superalloy, Metallurgical and Materials Transactions A 43 (2012) 1649–1661. ADS Bibcode: 2012MMTA...43.1649S.
15. T. Gabb, Comparison of [gamma-gamma] prime phase coarsening responses of three powder metal disk superalloys, NASA technical memorandum, National Aeronautics and Space Administration, Glenn Research Center, 2016.
16. G. Olson, H. Jou, J. Jung, J. Sebastian, A. Misra, I. Locci, D. Hull, Precipitation Model Validation in 3rd Generation Aeroturbine Disc Alloys, in: Superalloys 2008 (Eleventh International Symposium), TMS, 2008, pp. 923–932.
17. N. D'Souza, W. Li, C. Argyrakis, G. D. West, C. D. Slater, On the Evolution of Primary Gamma Prime Precipitates During High Temperature and High Strain Rate Deformation and Subsequent Heat Treatment in the Ni-Based Superalloy, RR1000, Metallurgical and Materials Transactions A 50 (2019) 4205–4222.
18. M.-A. Charpagne, P. Vennéguè, T. Billot, J.-M. Franchet, N. Bozzolo, Evidence of multimicrometric coherent γ' precipitates in a hot-forged γ – γ' nickel-based superalloy: Evidence of Multimicrometric Coherent, Journal of Microscopy 263 (2016) 106–112.
19. F. Bachmann, R. Hielscher, H. Schaeben, Texture Analysis with MTEX - Free and Open Source Software Toolbox, Solid State Phenomena 160 (2010) 63–68.
20. M.-A. Charpagne, T. Billot, J.-M. Franchet, N. Bozzolo, Heteroepitaxial recrystallization observed in René 65™ and Udimet 720™: A new recrystallization mechanism possibly occurring in all low lattice mismatch γ – γ' Superalloys?, Superalloys 2016: Proceedings of the 13th International Symposium on Superalloys 2016-January (2016) 417–426.
21. R. D. Doherty, Role of interfaces in kinetics of internal shape changes, Metal Science 16 (1982) 1–14.
22. J. W. Martin, R. D. Doherty, B. Cantor, Stability of Microstructure in Metallic Systems, Cambridge Solid State Science Series, Cambridge University Press, Cambridge, 2 edition, 1997.
23. Y. Chen, C. A. Schuh, Diffusion on grain boundary networks: Percolation theory and effective medium approximations, Acta Materialia 54 (2006) 4709–4720.
24. T. R. McNelley, M. E. McMahon, Microtexture and grain boundary evolution during microstructural refinement processes in SUPRAL 2004, Metallurgical and Materials Transactions A 28 (1997) 1879–1887.
25. R. E. García, M. D. Vaudin, Correlations between the crystallographic texture and grain boundary character in polycrystalline materials, Acta Materialia 55 (2007) 5728–5735.
26. A. Coyne-Grell, J. Blaizot, S. Rahimi, I. Violatos, S. Nouveau, C. Dumont, A. Nicolaÿ, N. Bozzolo, Recrystallization mechanisms and associated microstructure evolution during billet conversion of a gamma-gamma' nickel based superalloy, Journal of Alloys and Compounds 916 (2022) 165465.

27. S. Vernier, J.-M. Franchet, C. Dumont, P. Vennéguè, N. Bozzolo, γ' precipitates with a twin orientation relationship to their hosting grain in a $\gamma - \gamma$' nickel-based superalloy, Scripta Materialia 153 (2018) 10–13.
28. P. A. Manohar, M. Ferry, T. Chandra, Five Decades of the Zener Equation, ISIJ International 38 (1998) 913–924.